Available online at www.sciencedirect.com

SCIENCE DIRECT

Thin Solid Films 491 (2005) 190 – 196

thin solid films

www.elsevier.com/locate/tsf

Growth and characterization of Ti_xNi_{1-x} shape memory thin films using simultaneous sputter deposition from separate elemental targets

Sohrab Sanjabi [a,b,*], Sayed K. Sadrnezhaad [b], Karen A. Yates [a], Zoe H. Barber [a]

[a] Device Materials Group, Department of Materials Science and Metallurgy, Cambridge University, Pembroke Street, Cambridge CB2 3QZ, UK
[b] Department of Materials Science and Engineering, Sharif University of Technology, P.O. Box 11365-9466,Tehran, Iran

Received 17 November 2004; received in revised form 10 May 2005; accepted 3 June 2005
Available online 5 July 2005

Abstract

The fabrication of Ti_xNi_{1-x} shape memory films using simultaneous magnetron sputtering from two separate, elemental targets was investigated. The films were deposited at room temperature and then annealed at 500 °C to achieve the shape memory effect. The influence of sputtering parameters such as power ratio to the targets (to control the composition) and Ar gas pressure (to control the film structure) were studied. It was found that the Ar gas pressure had a critical influence on the shape memory effect of the films. Characterization of the films was carried out by energy dispersive X-ray spectroscopy in a scanning electron microscope (to measure the film composition and uniformity), in situ X-ray diffraction (to identify the phase structures) and differential scanning calorimetry (to indicate the transformation and crystallization temperatures). The results showed that, by controlling the power ratio to the Ti and Ni targets and the deposition geometry, the required film compositions (Ni-rich, equiatomic NiTi and Ti-rich) could be obtained. The evolution of the transformation temperatures is found to be qualitatively comparable to bulk material. The advantage of this method is the ability to control the film composition via control of target power.
© 2005 Elsevier B.V. All rights reserved.

Keywords: Sputtering; Shape memory alloy; TiNi; X-ray diffraction

1. Introduction

For more than a decade thin film shape memory alloys (SMAs) have been recognised as promising materials from which to make Micro-Electro-Mechanical Systems (MEMS) and Bio-MEMS microactuators (e.g. micropump [1], microwrapper [2] and stent for neurovascular blood vessels [3]), with many advantages over other materials due to the shape memory effect and superelasticity [4]. To utilize these properties, some factors need to be considered in view of fabrication and metallurgical processing, for example, control of composition and heat treatment. The composition adjustment is requisite to control the working temperature of the microdevices, since the phase transformation temperatures of NiTi alloys are sensitive to the composition ratio of Ti and Ni: only 1 at.% variation of composition can cause 100 °C shift in transformation temperature [5]. In addition to controlling film composition, other parameters, such as contamination during processing [6] (including oxidation of titanium which can result in loss of composition control) and compatibility with conventional microfabrication processing must be considered. Although a number of techniques have been used for depositing NiTi SMA thin films, such as sputtering [7], laser ablation [8], flash evaporation [9], and cathodic arc plasma ion plating [10], from the practical point of view, only sputter deposition has succeeded so far and the perfect shape memory effect similar to bulk materials can be obtained [7].

In sputtering, an alloy target is generally used and the compositions of the sputtered films are always Ni-rich in

* Corresponding author. Department of Materials Science and Engineering, Sharif University of Technology, P.O. Box 11365-9466, Tehran, Iran. Tel.: +98 21 6165315; fax: +98 21 6005717.
E-mail address: sanjabi@mehr.sharif.edu (S. Sanjabi).

0040-6090/$ - see front matter © 2005 Elsevier B.V. All rights reserved.
doi:10.1016/j.tsf.2005.06.004

comparison with the target (the films are Ti poor with respect to the target (by 2–4 at.%)) because the sputtering yield for Ni is higher than Ti [11]. The simplest and most common solution to this problem is to place small pieces of pure Ti onto the target, to achieve the correct film stochiometry [7]. Alternatively this can be achieved by co-sputtering of the alloy target with a pure Ti target [12], using an alloy target enriched in Ti [13] or varying the working gas pressure in the chamber. However, it is difficult to adjust the composition by varying Ar gas pressure, because at high pressures films become brittle, with poor structure [14]. Target modification also requires a trial and error approach to produce the correct film composition: the composition adjustment using Ti (or Ni) plates requires control of numerous parameters such as number, geometry, size and position, and any subsequent change of the deposition parameters will require re-adjustment. Manufacturing of the required alloy targets from investment casting or powder metallurgy requires control of impurities such as oxygen, or pre-alloyed powder impurities [15]. In order to obtain homogeneous sputtered films, powder metallurgical targets must consist of relatively small but well-mixed powders of elements. This technique leads to high impurity levels due to the large surface contribution. Also, the production of cast-melted targets, a reliable alternative in terms of achieving lower levels of oxygen impurities, needs high vacuum conditions. This is most important as oxygen impurities have an effect on phase transformation and ductility [16].

The control of film composition from separate targets, controlled by the power ratio, is more flexible and can overcome these problems. The control of composition uniformity is important, requiring appropriate deposition geometry (e.g. inclining the axes of the targets [17], and optimizing the substrate-target distance, and size and shape of targets). Krulevitch et al. used a Direct Current (DC) magnetron system to sputter from individually powered Ni, Ti, and Cu targets without substrate rotation leading to a large variation of composition [18]. Lehnert et al. fabricated films by multilayering of Ni and Ti (around 50 bilayers, each consisting of 10 nm Ni and 19 nm Ti) [19] and Ohta et al. deposited a multilayer film using high-speed substrate rotation to reduce the layers below 1 nm [20]. Fabrication of alloy films from multilayers may require higher crystallization temperature and not be compatible with conventional microfabrication.

In this study shape memory Ni-rich, equiatomic NiTi, and Ti-rich films were fabricated by simultaneous sputter deposition from separate elemental Ni and Ti targets (mixing of elements before arrival at the substrate) and annealing at a relatively low temperature. Film properties were comparable with NiTi bulk material. One important advantage of this fabrication method is the ability to produce films with any required composition by adjusting the power to each target.

2. Experimental details

Films were deposited by ultra high vacuum DC magnetron sputtering onto unheated Si (100) substrates with a dimension of 10×5 mm. The substrates were placed across the diameter of a circular substrate holder to explore the composition uniformity as a function of position. A base vacuum of $<1 \times 10^{-6}$ Pa was achieved after overnight bake-out and subsequent liquid nitrogen cooling of the chamber walls. The deposition system allows two or three magnetrons (target size: 35×55 mm), plus associated heater leads, instrumentation feed-throughs, viewing port and rotary shaft to be placed on one standard 200 mm OD flange, inserted into a 150 mm ID nitrogen-cooled can [21]. Configuration of the flange used in this study included two separate elemental targets (Ni and Ti with a purity of 99.9%) and a substrate holder which could be rotated in the horizontal plane in order to achieve a uniform film composition (Fig. 1). The substrate holder was rotated at 10 rpm during sputtering. A constant flow of Ar (99.999%) was controlled with a leak valve during film deposition, and different sputtering gas pressures were achieved by throttling the gate valve.

Thickness of the films was measured by surface profilometry (Talysurf 6, Taylor-Hobson) using the step height on a masked silicon substrate: the deposition rate was calculated to be about 1 μm/h; the thickness of the films was around 2 μm. As-deposited films were annealed at 500 °C for 1 h in a vacuum furnace (base pressure $<1 \times 10^{-5}$ Pa) with heating and cooling rates of approximately 50 °C/min. The composition of as deposited films was determined by energy dispersive X-ray spectroscopy using a JEOL JSM-5800LV operating at 15 keV. Films were examined by observing fracture cross-sections in a Field Emission Scanning Electron Microscope (FESEM) using a JEOL JSM-6340F.

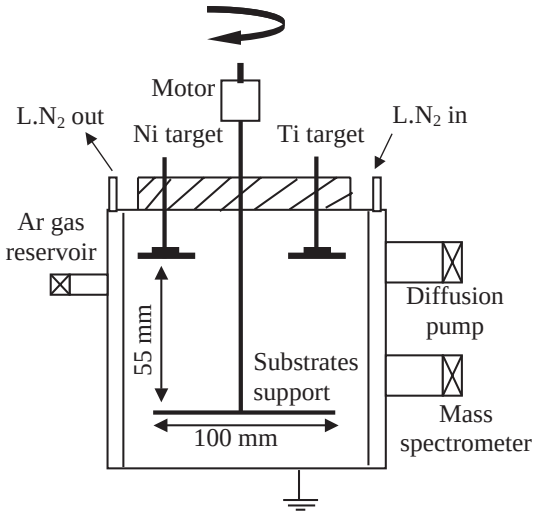

Fig. 1. Schematic illustration of the sputtering configuration.

For X-ray diffraction (XRD) a Philips PW1060 with Cu-Kα (λ=1.54056 Å) X-ray source was used to identify the film structure as a function of temperature. Differential Scanning Calorimetery (DSC) (Q1000, TA instrument, with the minimum required mass=0.5 mg) was used to indicate the crystallization temperature and transformations at heating and cooling rates of 10 °C/min. A four-point electrical resistivity measurement was also used to characterize the shape memory hysteresis of the films and measure the transformation temperatures.

3. Results and discussion

Without substrate rotation, suitable powers were applied to each target to give similar deposition rates (of Ni and Ti) at the center of the substrate support. Fig. 2a shows the resulting composition variation across the substrate support (power ratio of Ti to Ni was around 3). By using substrate rotation, composition uniformity was achieved across the diameter of the substrate holder. Fig. 2b shows the composition variation for different composition ranges (Ni-rich, near equiatomic and Ti-rich films). The composition uniformity was affected by deposition geometry. For example a small deviation of the substrate holder from the horizontal plane led to around 1 at.% variation across the 100 mm substrate holder diameter (0.01 at.%/mm).

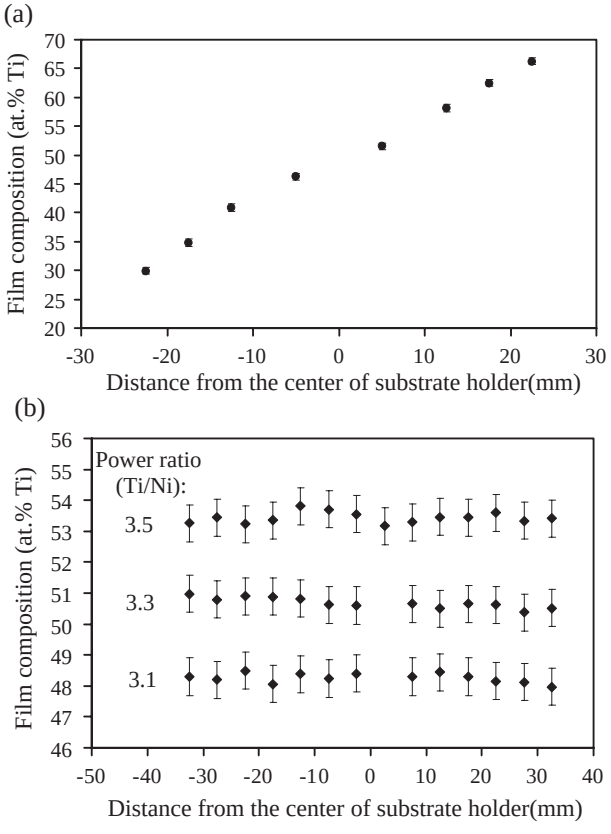

Fig. 2. The composition variation across the substrate holder using (a) stationary, and (b) rotating substrate holder (for 3 different target power ratios).

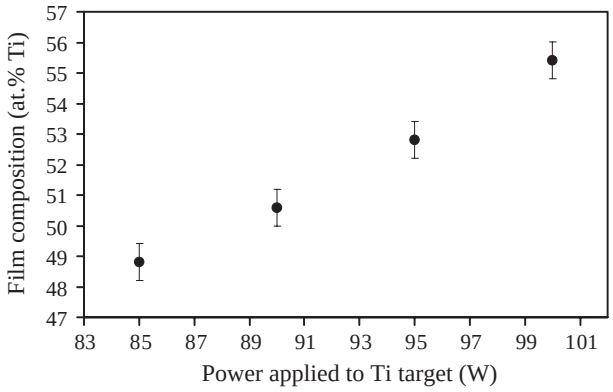

Fig. 3. Dependence of the film composition on the applied power (power to Ni target=27W).

Required film compositions were obtained by changing the power to the Ti target whilst the Ni power was kept constant (at 27 W). Fig. 3 shows the dependence of film composition on the applied Ti power at a constant Ar gas sputtering pressure of 0.6 Pa and target-substrate distance of 55 mm (using rotating substrate support).

Important parameters which affect the quality of the films are target power (and hence the deposition rate), Ar gas pressure, substrate-target distance, substrate temperature, and purity of the targets and the deposition environment. The Ar pressure and the target-substrate distance affect the energies of the depositing species and hence film density, structural integrity and stress. At high Ar pressures films often show low density, containing structural defects, whilst at low pressures the structure is denser with fewer defects [22]. Films spanning a range of compositions, prepared at high Ar pressures (>1 Pa) had a brittle structure and cracks were observed on the film surface: Fig. 4a shows the extensive delamination at the NiTi/Si interface and cracks caused by in-plane, biaxial tensile stresses. This figure also reveals a wavy fracture morphology, indicating that the interface cracks have penetrated into the Si substrate near the NiTi/Si interface, implying that the interface toughness is greater than the bulk toughness of the single crystal silicon substrate [12]. Films covering a similar range of composition, prepared at low Ar pressures exhibited a smooth, featureless surface structure: Fig. 4b shows the cross-section of a film deposited at 0.6 Pa.

XRD of as-deposited films showed only a broad peak around 2θ=42° and no crystalline peaks, suggesting an amorphous structure (see Fig. 5.). After annealing, in spite of similar composition, films deposited at two different gas pressures showed very different film structures. The XRD spectrum of a 51.2 at.% Ti, film deposited at 1.2 Pa (see Fig. 5a.), showed only austenite phase (peaks at 42.7° and 62°, corresponding to 110 and 200 austenite reflections) at room temperature. The shape memory effect of this film was characterized by electrical resistivity as a function of

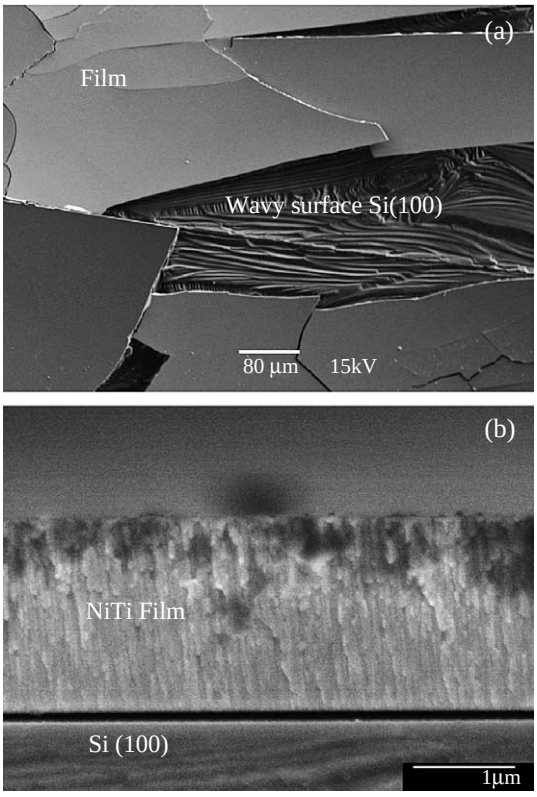

Fig. 4. Scanning electron micrographs of films deposited at different Ar gas pressures: (a) plan view of a film deposited at 1.2 Pa, showing severe surface delamination, and (b) FESEM cross-section of a film deposited at 0.6 Pa.

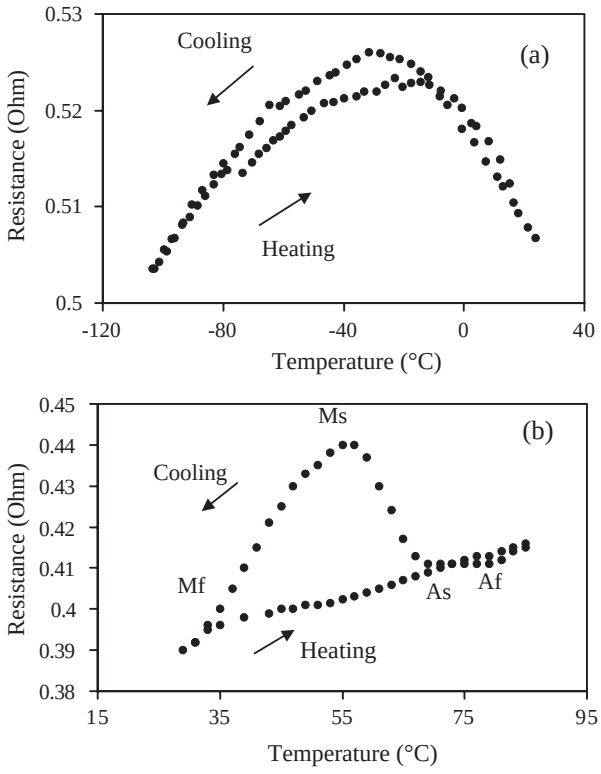

Fig. 6. Electrical resistivity measurement as a function of temperature for films deposited at different Ar gas pressures and annealed at 500 °C: (a) 1.2 Pa with composition of $Ti_{51.2}Ni_{48.8}$ and (b) 0.6 Pa with composition of $Ti_{50.6}Ni_{49.4}$.

temperature, see Fig. 6a, confirming that the transformation temperature of this film is below room temperature. The loop of shape memory during cooling and heating is not clear, and one peak can be observed around −40 °C. Following deposition of a similar film composition at a lower Ar pressure (0.6 Pa) the annealed film showed martensite peaks in the room temperature XRD spectrum, Fig. 5b (see below for indexing of these peaks). The existence of the martensite peaks at room temperature indicates that the shape memory effect and phase transformation occur above room temperature, as confirmed by the electrical resistivity measurement shown in Fig. 6b. These results illustrate that, in spite of controlling the film composition, poor shape memory effect was observed in films deposited at high pressure.

An essential feature of sputtered film structures is that they are formed from a flux that approaches the substrate from a limited set of directions and consequently the grains tend to be columnar. Furthermore, for low temperature

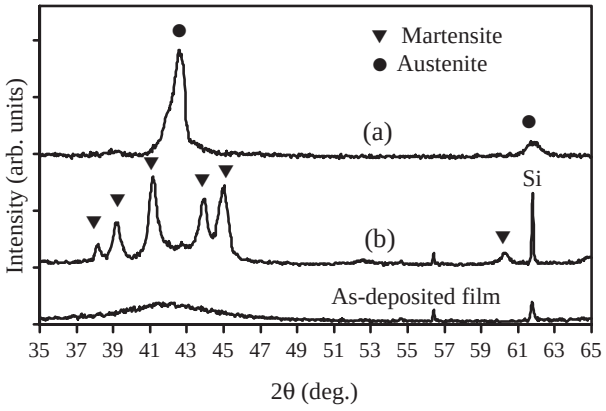

Fig. 5. Room temperature XRD profiles of films deposited at different Ar gas pressures (annealed at 500 °C): (a) 1.2 Pa with composition of $Ti_{51.2}Ni_{48.8}$ and (b) 0.6 Pa with composition of $Ti_{50.6}Ni_{49.4}$ (see later text for indexing of peaks). XRD of an as-deposited film is also shown.

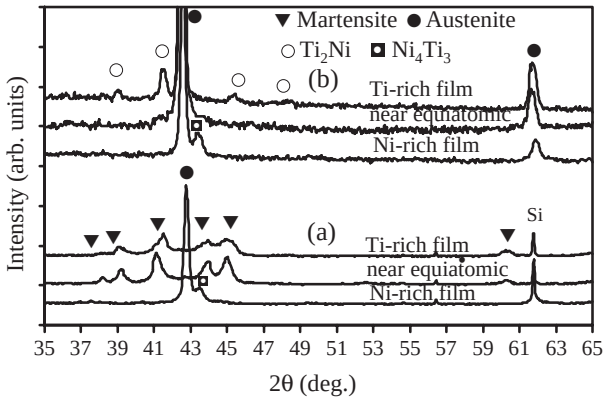

Fig. 7. XRD trace of Ti-rich ($Ti_{52.8}Ni_{47.2}$), near-equiatomic ($Ti_{50.6}Ni_{49.4}$) and Ni-rich ($Ti_{48.8}Ni_{51.2}$) films annealed at 500 °C at (a) room temperature, and (b) 100 °C (see text for indexing of peaks).

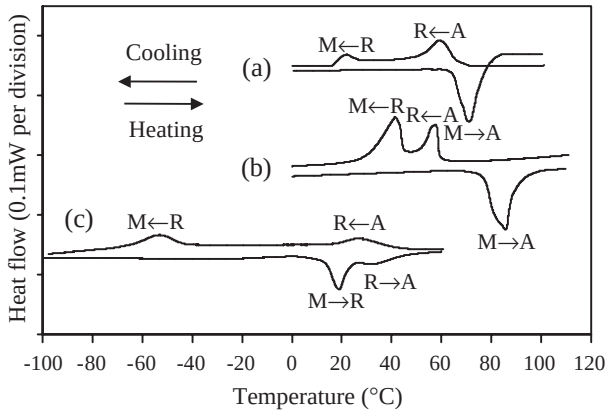

Fig. 8. DSC curves of (a) Ti-rich ($Ti_{52.8}Ni_{47.2}$) (b) near-equiatomic ($Ti_{50.6}Ni_{49.4}$), and (c) Ni-rich ($Ti_{48.8}Ni_{51.2}$) films annealed at 500 °C.

deposition (i.e. room temperature) a growth structure defined by voided boundaries (also columnar) is superimposed on the intrinsic grain structure in the film. Thus, thin film microstructures tend to have an anisotropic character, which influences the film properties. The voided growth defects are a consequence of atomic shadowing, which is influenced by parameters such as deposition geometry, Ar gas pressure, and substrate surface roughness [22]. Increase of the Ar gas pressure enhances the oblique component in the deposition flux due to increased gas scattering, which promotes shadowing and reduces the density of the film.

In addition to poor film structure in films deposited at high pressures, which may suppress the transformation, the shape memory effect is also influenced by the annealing temperature used. Ishida et al. have reported that relatively low temperature annealing (500 °C, as used here) in slightly Ti-rich films led to a reduced transformation temperature, below room temperature, due to the formation of GP zones. A higher annealing temperature (e.g. 600 °C) may therefore overcome this effect [23].

Thin films with different compositions were fabricated at the Ar gas pressure of 0.6 Pa and then annealed at 500 °C for 1 h. After annealing the films showed different crystalline phase structures. Fig. 7 shows the XRD traces of annealed Ni-rich, near equiatomic, and Ti-rich films at room temperature and 100 °C.

For an equiatomic NiTi film at room temperature, diffraction patterns showed peaks at 2θ=(38.2°, 39.1°, 41.3°, 44.05°, 45.1°, 60.2°), indexed as 110, 002, −111, 020, 012, and 022 planes, respectively, of the B19′ (monoclinic) martensite structure, Fig. 7a. During heating to 100 °C the martensite peaks gradually disappeared and were replaced by a sharp peak at 2θ=42.7° and a minor peak at 2θ=62°, Fig. 7b, which corresponds to austenite 110 and 200.

The diffraction pattern of the Ti-rich film is similar to the near equiatomic film, although some precipitation such as Ti_2Ni can be observed. It has been reported that during crystallization the Ti_2Ni precipitates nucleate and grow along the austenite grain boundaries due to the high concentration of Ti [24]. The peaks due to Ti_2Ni are very close to the martensite peaks in the range of 2θ=37°–47° and are difficult to identify at room temperature. At higher temperatures (>100 °C), there is some evidence of Ti_2Ni precipitation around the sharp austenite peak at 2θ=42.7° and on further increasing temperature, these peaks did not change. The peaks associated with this phase occur at 2θ=(38.9°, 41.4°, 45.3°, 47.5°), indexed as 422, 511, 440, 531 (shown in Fig. 7b).

In a Ni-rich film, at room temperature, a large peak at 2θ=42.7° along with a smaller peak at 2θ=61.2° correspond to reflections from 110 and 200 planes of the B2 (CsCl-type) austenite phase structure. In this figure also a small peak at 2θ=43.4° is observed. The higher temperature XRD illustrates that after increasing the temperature to 100 °C, the position of this peak does not change (see Fig. 7b). According to the XRD data source (39-1113) this peak may correspond to the 122 peak of Ni_4Ti_3. This precipitation has been reported in the matrix of Ni-rich thin films following short annealing processes [25]. The XRD results illustrate that there is no precipitation in near equiatomic films, whilst there is in both the Ni- and Ti-rich.

Annealed NiTi thin films undergo a martensitic phase transformation when cooled below their transformation temperature. DSC measurement was performed on the films under heating and cooling at a rate of 10 °C/min over a wide range of temperature (−150 to 150 °C). In this case the films (with dimension 2 μm × 5 mm × 10 mm) were removed from the substrate giving a mass of around 0.5–0.6 mg. Fig. 8 shows the DSC curves during heating and cooling for films with different compositions: (a) Ti-rich, (b) near-equiatomic and (c) Ni-rich. The corresponding transformation temperatures are summarized in Table 1.

Table 1
Phase transformation temperatures and transformation enthalpy as a function of film composition

Film composition	Heating						Cooling					
	R_s (°C)	R_f (°C)	$\Delta H_{M\to R}$ (J/g)	A_s (°C)	A_f (°C)	$\Delta H_{M\to A}$ (J/g)	R_s (°C)	R_f (°C)	$\Delta H_{A\to R}$ (J/g)	M_s (°C)	M_f (°C)	$\Delta H_{R\to M}$ (J/g)
Ti-rich ($Ti_{52.8}Ni_{47.2}$)				64	78	17.3	65	50	5.8	27	11	4.5
NiTi ($Ti_{50.6}Ni_{49.4}$)				71	86	22.3	58	46	5.9	44	26	14.3
Ni-rich ($Ti_{48.8}Ni_{51.2}$)	13	27	5.28	27	44	1.4[a]	40	13	4.1	−42	−71	5.9

[a] In the Ni-rich film this number is corresponded to $\Delta H_{R\to A}$.

The transformation temperatures of near equiatomic and Ti-rich films are above room temperature whilst that of the Ni-rich film is lower. In Fig. 8b, which shows the DSC results of the near equiatomic NiTi film, a one-stage transformation is observed during heating, corresponding to B19′ to B2 transformation. The transformation enthalpy of 22.3 J/g confirms that this peak is related to a direct transformation from martensite to austenite phases: the transformation starts from 71 °C and finishes at 86 °C. During cooling, a two-stage transformation is observed, corresponding to transformation between B2, R-phase and B19′ phases. The austenite phase starts to transform to R-phase at around 60 °C. The R-phase starts to change to the martensite phase at a temperature around 50 °C and finishes at 30 °C. This evaluation indicates that the martensite structure is dominant at room temperature and austenite at higher temperature (around 100 °C), as indicated by XRD, Fig. 7.

The transformations of the Ti-rich film are similar to the near equiatomic NiTi film (Fig. 8a), except that the temperatures are lower and there is a wide temperature range in transforming between $A \rightarrow R$ and $R \rightarrow M$ on cooling. During heating the martensite to austenite transformation occurs from 65 to 80 °C and during cooling the R-phase starts at a temperature around 65 °C and finishes at 50 °C. By further cooling, the R-phase transforms to martensite at around 25 °C. During cooling this transformation is not completed and the XRD peaks related to R-phase can be observed at room temperature after one thermal cycling. Results show that the transformation in Ti-rich thin films is not stable and during heating and cooling the transformation shifts to lower temperatures. The precipitates and fine grain size may suppress the martensite transformation [23,24].

DSC curves of the Ni-rich film, Fig. 8c, show a two-step transformation both during heating and cooling. Depending on the annealing temperature and time and the composition either a two-stage or one-stage transformation occurs in Ni-rich films [25]. In Table 1, in addition to transformation temperatures, the energy for each phase transformation is included. From transformation temperatures, it can be seen that there is a hysteresis of around 50 °C for Ti-rich, 35 °C for near equiatomic and more than 90 °C for Ni-rich films between the austenite formation during heating and the martensite transformation during cooling.

The temperature range for annealing of the films was evaluated by DSC. For these measurements the as-deposited films were removed from the Si substrates in the amorphous state and then heated up to a temperature around 600 °C with a constant rate of 10 °C/min. Fig. 9 shows the heat flow as a function of temperature for a near-equiatomic film composition. It can be seen that the crystallization temperature is around 472 °C. The corresponding reaction enthalpy is 29 J/g. These results show that there is no difference between these data and typical DSC crystallization curves of conventional sputtered NiTi thin films [19]. Also it confirms that the selection of low annealing temperature around 500 °C is sufficient to crystallize the films reported here.

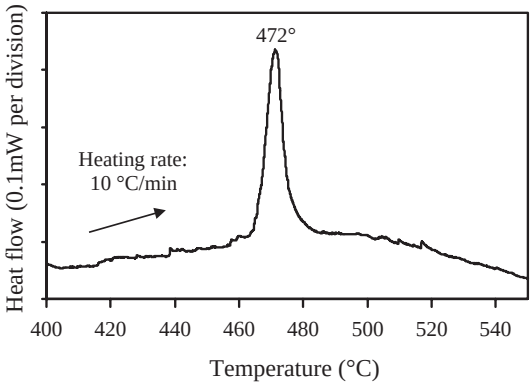

Fig. 9. DSC trace of crystallization temperature of as-deposited near-equiatomic NiTi film.

4. Conclusion

The fabrication of shape memory Ti_xNi_{1-x} thin films using simultaneous sputter deposition from separate elemental targets was demonstrated. The influence of the sputtering parameters on the quality of the film and shape memory effect has been illustrated: in spite of composition control, at higher Ar gas pressure the transformation temperature can occur below room temperature and the shape memory hysteresis loop during heating and cooling is not clear. Following deposition at low gas pressure phase transformations showed a qualitatively similar behaviour as a function of film composition to Ni-Ti bulk materials. The significant parameters in this process are the control of deposition geometry, relative powers to each target, working gas pressure, and substrate–target distance.

Simultaneous sputter deposition from two targets offers flexibility in control of the required composition and it is simple to add another target for fabrication of ternary shape memory thin films.

Acknowledgements

The authors would like to thank David Vowles (electron microscopy), Andrew Moss (X-ray diffraction), and Robert Cornell (polymer characterisation) in the department of Materials Science and Metallurgy, University of Cambridge.

References

[1] D. Xu, L. Wang, G. Ding, Y. Zhou, A. Yu, B. Cai, Sens. Actuators, A, Phys. 93 (2001) 87.
[2] J.J. Gill, D.T. Chang, L.A. Momoda, G.P. Carman, Sens. Actuators, A, Phys. 93 (2001) 148.
[3] V. Gupta, V. Martynov, A.D. Johnson, Actuator 2002 (2002) 355.

[4] Y. Fu, H. Du, W. Huang, S. Zhang, M. Hu, Sens. Actuators, A, Phys. 112 (2004) 395.
[5] K.N. Melton, in: T.W. During, K.N. Melton, D. Stockel, C.M. Wayman (Eds.), Engineering Aspects of Shape Memory Alloys, Butterworth-Heinemann, London, UK, 1990, p. 23.
[6] K. Ikuta, H. Fujishiro, M. Hayashi, T. Matsuura, Proceedings of the First International Conference on Shape Memory and Superelastic Technologies, Asilomar Conference Center, Pacific Grove, California, USA, 1994, p. 13.
[7] S. Miyazaki, A. Ishida, Mater. Sci. Eng., A Struct. Mater.: Prop. Microstruct. Process. 273–275 (1999) 106.
[8] X.Y. Chen, Y.F. Lu, Z.M. Ren, S. Zhu, J. Mater. Res. 17/2 (2002) 279.
[9] E. Makino, M. Uenoyama, T. Shibata, Sens. Actuators, A, Phys. 71 (1998) 187.
[10] J.L. He, K.W. Won, J.T. Chang, Thin Solid Films 359 (2000) 46.
[11] D.S. Grummon, L. Hou, Z. Zhao, T.J. Pence, J. de. Phys. IV 5 (1995) 665.
[12] C.L. Shih, B.K. Lai, H. Kahn, S.M. Philips, A.H. Heuer, J. MEMS 10 (2001) 69.
[13] E. Quandt, C. Halene, H. Holleck, K. Feit, M. Kohl, P. Schlomacher, A. Skokan, Sens. Actuators, A, Phys. 53 (1996) 434.
[14] A. Ishida, A. Takei, S. Miyazaki, Thin Solid Films 228 (1993) 210.
[15] H. Rumpf, B. Winzek, C. Zamponi, W. Siegert, K. Neuking, E. Quandt, Mater. Sci. Eng., A Struct. Mater.: Prop. Microstruct. Process. 378 (2004) 429.
[16] T. Saburi, in: K. Otsuka, C.M. Wayman (Eds.), Shape Memory Materials, Cambridge University Press, United Kingdom, 1998, p. 72.
[17] T. Yamamoto, S. Miyazaki, J. de Phys. IV 112 (2003) 869.
[18] P. Krulevitch, P.B. Ramsey, D.M. Makowiecki, A.P. Lee, M.A. Northrup, G.C. Johnson, Thin Solid Films 274 (1996) 101.
[19] T. Lehnert, H. Grimmer, P. Boni, M. Horisberger, R. Gotthardt, Acta Mater. 48 (2000) 4065.
[20] A. Ohta, S. Bhansali, I. Kishimoto, A. Umeda, Sens. Actuators, A, Phys. 86 (2000) 165.
[21] R.E. Somekh, Z.H. Barber, J. Phys., E J. Sci. Instrum. 21 (1988) 1029.
[22] J.A. Thornton, J. Vac. Sci. Technol., A, Vac. Surf. Films 4 (6) (1986) 3059.
[23] A. Ishida, M. Sato, T. Kimura, T. Sawaguchi, Mater. Trans. 42 (2001) 1060.
[24] S. Kajiwara, K. Ogawa, T. Kikuchi, T. Matsunaga, S. Miyazaki, Philos. Mag. Lett. 74 (1996) 395.
[25] A. Gyobu, Y. Kawamura, H. Horikawa, T. Saburi, Mater. Sci. Eng., A Struct. Mater.: Prop. Microstruct. Process. 273–275 (1999) 749.